Chemistry–A European Journal
Communication
doi.org/10.1002/chem.202103351
Chemistry Europe
European Chemical Societies Publishing
www.chemeurj.org

Catechol Moiety Integrated Tri-Aryl Type AIEgen for Visual and Quantitative Boronic Acid Detection

Renjian Hu[+],[a] Shiyun Lin[+],[b] Mengshi Wang,[a] Ruoxin Li,[a] Zhigang Shuai,[b] and Yen Wei*[a, c]

Abstract: Novel functional AIEgen based on three compact bound aryl skeletons is designed and synthesized. This tri-aryl type luminogen (TA-Catechol) embedded with catechol moiety responds rapidly to series of boronic acids. Real-time visual and quantitative dual-mode detection method is established for the first time with modest precision and low detection limit (8.0 μM). Detailed mechanistic discussion identifies tetra-coordinated boronic species as the key intermediate within sensing procedure. Wide range of organic boronic acids compatible with this strategy is displayed which is promising in high throughput screening technology. Furthermore, solid-state sensing capability of TA-Catechol is also demonstrated.

Introduction

Organoboron chemistry is a cask of aging wine among the family of Main Group Chemistry. Early discovery of hydroboration reaction within the 1950s provokes convenient synthesis of series organoboron compounds especially organoboranes.[1] With the landmark exploration of transition metal catalyzed cross-coupling reaction between organoboron compound and organohalide which is later known as Suzuki-Miyaura reaction since the 1970s,[2] chemists come to realize the versatility of organoboronic species in organic synthesis. Nowadays, organoboronic species including boronic acids and boronic esters have inspired enormous research interest through interdisciplinary manner.[3] Numerous methodologies involving preparation and transformation of boronic species have been exploited recent years.[4] Besides, utilization of small-molecules with boronic acid group as pharmaceuticals[5] and state-of-the-art therapeutic agents[6] becomes more and more reliable. It also plays pivotal role in Analytical Chemistry and Material Science for saccharide detection[7] or hydrogel architecting.[8] For the widespread scenario where boronic acids are exploited, development of operative detection methods for boronic acids are of great significance. Previous reported methods spanning mass spectrometry,[9] membrane potential approach[10] and photoluminescent procedure.[11] They either require sophisticated manipulations[9–10,12] or just hold singular mode.[11] Thus, establishment of a convenient and highly-efficient boronic acid detection method is in urgent demand.

1,8-Diarylsubstituted naphthalene moiety is a time-honored scaffold with three tightly linked aryl groups and relative research efforts could be traced back to the 1960s.[13] Since then, investigation of atropisomerism[14] while determination of rotational barrier[15] towards the pair of peri-substituted (hetero) aryl groups is systematically carried out. With feasible modification of the peri sites of the naphthalene skeleton, interaction between the pair of (hetero)aryl groups could be interrogated comprehensively.[16] Scientists have also established several types of frustrated Lewis acid-base pairs based on this structure.[17] Furthermore, Wolf's group has been devoted to the fundamental chemistry and practical applications of 1,8-diarylsubstituted naphthalene based fluorescence sensors since 2003.[18] Series of fluorescence probes come to be developed for the detection of ions and chiral molecules with good to excellent performances these years.[19] However, fluorescence sensor with both visual and quantitative detection modes is scarcely reported to date.

Development of fluorescent sensors based on aggregation-induced emission (AIE) mechanism overcomes conventional self-quenching effect in the solid-state and brings about multiple advantages such as high sensitivity, large detection range and visualized sensing process.[20] Inspired by the intrinsic functionalization strategy proposed by our group for the rational design of AIE luminogen,[21] we construct the functional tri-aryl type AIEgen bearing catechol moiety with visual and quantitative detection modes towards boronic acids for the first time. Detailed structural and spectroscopic properties are thoroughly analyzed and established. Tetra-coordinated luminescent boronic species is identified as the key intermediate through the detection procedure both experimentally and theoretically. Detection limit (LOD) of this probe is determined

[a] R. Hu,[+] M. Wang, Dr. R. Li, Prof. Y. Wei
The Key Laboratory of Bioorganic Phosphorus Chemistry & Chemical Biology
Department of Chemistry
Tsinghua University
Beijing 100084 (P. R. China)
E-mail: weiyen@tsinghua.edu.cn

[b] S. Lin,[+] Prof. Z. Shuai
MOE Key Laboratory of Organic Optoelectronics and Molecular Engineering
Department of Chemistry
Tsinghua University
Beijing 100084 (P. R. China)

[c] Prof. Y. Wei
Department of Chemistry
Center for Nanotechnology and Institute of Biomedical Technology
Chung-Yuan Christian University
Chung-Li 32023, Taiwan (P. R. China)

[+] These authors contributed equally to this work.

Supporting information for this article is available on the WWW under https://doi.org/10.1002/chem.202103351

as 8.0 μM and the visual resolution limit almost approaches 10 μM, which are among the best values in comparison with previous reports up to date. Rapid, precise and convenient characteristics of this responsive luminogen endow it with great potential in high throughput screening (HTS) and drug metabolism research.

Results and Discussion

Synthesis and characterization

The synthetic procedure for **TA-Catechol** is briefly demonstrated in Figure 1. We begin our synthesis with two-step cascaded *Suzuki-Miyaura* coupling to obtain the methyl protected **TA-Catechol** with moderate total yield of 31.3%. The deprotection of the catechol moiety is carried out with BBr_3 in anhydrous DCM to afford **TA-Catechol** in 94.9% yield. $^1H/^{13}C$ NMR Spectroscopy, HRMS and FTIR provide basic compositional and structural information of our target molecule as well as several synthetic intermediates. Detailed processes and characterization data are provided in Supporting Information.

Slow evaporation of DCM solution with **TA-Catechol** affords colorless prismatic crystal. X-ray single crystal Diffraction experiments establish the geometric configuration and packing structure of **TA-Catechol** in the crystalline state (CCDC No. 2077157). As shown in Figure 2a, two enantiotropic molecules constitute the basic repetitive unit and triclinic system is taken by **TA-Catechol** single crystal with $P\bar{1}$ space group in general. *Peri*-substituted phenyl group takes a dihedral angle of 64.958° with the naphthalene ring and the dihedral angle between catechol moiety and naphthalene plane is determined to be 62.313°. Torsion angle of 15.991° exists between two *peri*-substituted groups which suppress the effective intramolecular π-π interaction at solid-state. The packing structure is expressed from the perspective view along **b** axis in Figure 2b. Intermolecular hydrogen bonds with interaction length of 1.994 Å, 1.877 Å, 2.157 Å and 2.271 Å are identified with additional C–H…π interaction between the *peri*-substituted phenyl C–H bond and the naphthalene π system. Two binding modes with interaction length of 2.848 Å and 3.000 Å are pointed out. These weak intermolecular interactions build up the fundamental skeleton in the solid-state of **TA-Catechol** which may bring about novel photophysical behavior under aggregation.

Basic spectroscopic properties

Ground state spectroscopic behavior of **TA-Catechol** is revealed with UV-vis spectra in THF solution (Figure S16). Maximum absorption peak at 299.8 nm is identified which indicated the existence of slight conjugation between naphthalene ring and the *peri* phenyl substituents within TA-Catechol. Fluorescence spectroscopy are employed to investigate its excited state properties. The determine the maximum emission wavelength

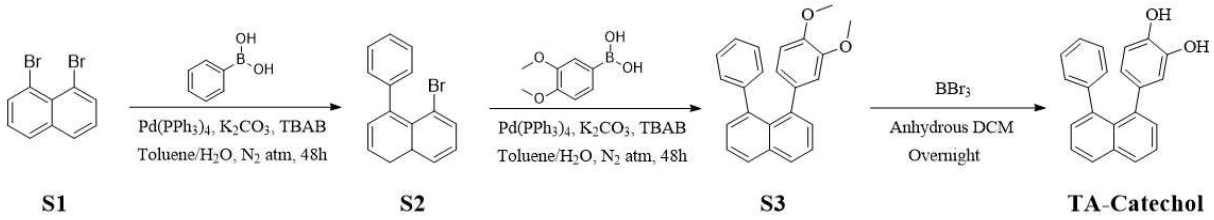

Figure 1. Scheme of synthetic procedure for **TA-Catechol**.

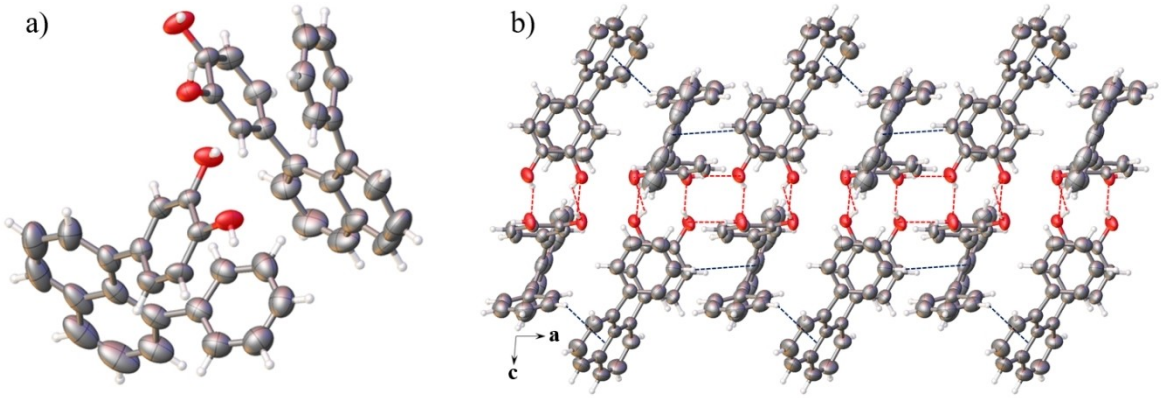

Figure 2. X-ray single crystal diffraction results of **TA-Catechol**. a) Molecular conformation of **TA-Catechol** at crystalline state. b) Packing structure of **TA-Catechol** molecules with perspective view from **b** axis. The dash lines indicate intermolecular interactions within crystal structure. (Noted that gray sphere represents carbon atom, red sphere represents oxygen atom and white sphere represent hydrogen atom).

is found to be 420 nm in THF solution with excited wavelength of 299.8 nm. As THF/H_2O is used as binary solvent and increasing the water fraction (f_w), molecular aggregation forms which could be monitored with SEM (Figure S18). The photoluminescence (PL) intensity of **TA-Catechol** with growing water fraction manifests a typical AIE feature as shown in Figure 3a–c. As the initial addition of DI water, the PL intensity damps rapidly with bathochromic shifted maximum emission wavelength. Excited-state proton transfer[22] brings about intermolecular weak conjugation and an additional energy dissipation pathway may account for this phenomenon. Subsequently, PL intensity proceeds mild decline with elevated f_w until it reached 70%. The fluorescence intensity boosts accompanied by hypochromatic shifted maximum emission wavelength with f_w approaching 99%. This could be attributed to the domination of aggregation process at f_w higher than 70% and the twist of molecular conformation along with it. The photoluminescent quantum yield measurement of **TA-Catechol** in solution (0.72%) and crystal (14.58%) further verifies its AIE behavior.

Theoretical calculations have been exploited to gain deep insights into the AIE mechanism for **TA-Catechol**. Density functional theory (DFT) and Time dependent DFT (TD-DFT) calculations are carried out by using the widely used B3LYP functional with dispersion-correction D3 and 6–31G(d,p) basis set for target molecule with polarizable continuum model (PCM) and ONIOM model by Gaussian 16.[23] (Detailed computational procedure are given in **Supporting Information**) The electronic structures, including main frontier molecular orbitals, their energy level and transition property are given in Figure 3d at optimized S_1 geometries in solution and crystal. It can be seen that the main transitions change from single HOMO→LUMO (98.2%) excitation in solution to hybrid HOMO→LUMO (93.6%) and HOMO-1→LUMO (5.2%) excitation in crystal. Consequently, the vertical excitation energy increases from 2.85 eV to 3.26 eV due to the participation of the deeper orbital in solid-state, which is confirmed by the hypochromatic shift of the emission spectrum related to that in solution observed in experiment.

We calculated the vibrationally resolved emission spectra at 298 K in solution and solid phase by using the thermal vibration correlation function theory via MOMAP program,[24] as plotted in Figure S30. Experimental emission spectrum is presented for comparison. We find that the calculated spectrum matches well with the experimental ones and the hypochromatic shifted maximum emission wavelength at aggregate state is reproduced with computational procedure.

The calculated radiative and nonradiative decay rate constants in solution and solid phase obtained from MOMAP

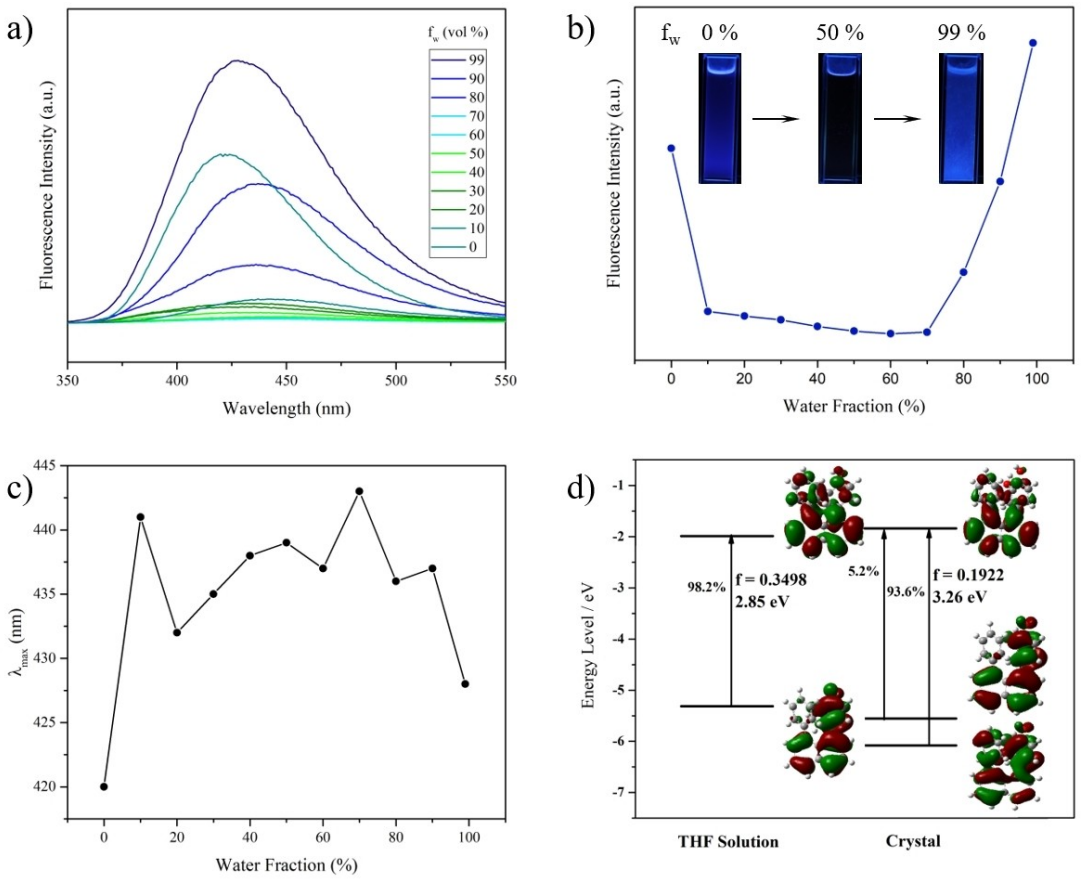

Figure 3. Photoluminescent behavior of **TA-Catechol** and illustrations. a) Fluorescence spectrum of **TA-Catechol** in THF/H_2O binary solvent with varying water fraction. b) Fluorescence intensity of **TA-Catechol** at 420 nm with different water fractions. c) Plot of maximum emission wavelength versus water fraction. d) Selected frontier molecular orbitals and important transitions of the S_1 state at optimized S_1 geometries in solution and crystal of **TA-Catechol**.

are given in Table S3, as well as the adiabatic excitation energy based on the geometries of S_1 states. As shown in Table S3, experimental radiative decay rate constant exhibits about 40 times increase from solution to solid phase while the non-radiative rate constant almost keeps invariant. And this trend is reproduced well with our theoretical method. The calculated photoluminescence quantum yield (PLQY) increases from 3.21% to10.01% upon aggregation, which agrees well with our experimental results.

To understand the AIE mechanism in this system in depth, we extract two important factors (reorganization energy and nonadiabatic coupling) to manipulate the non-radiative rate constant. As shown in Figure S31, the total reorganization energies decrease greatly from solution (6735.89 cm^{-1}) to solid state (3529.76 cm^{-1}), which contributes to the suppression of non-radiation process. From Figure S32, we can find that the largest contributions to the reorganization energy come from several low vibration modes, which could be basically attributed to the rotation of two phenyl groups. Similarly, the non-adiabatic couplings become much smaller from solution to solid state due to the restricted rotation of phenyl groups in solid-state.

Dual-mode boronic acid detection

Catechol moiety is extensively involved in the field of bioengineering and biomimetic materials for its flexible chelation approaches towards metal ions or boronic species.[25] Inheriting the chemistry of catechol segment, our synthetic luminogen might exhibit potential sensing capability for boronic acids. Initial attempt to compare the PL spectra of **TA-Catechol**/ phenylboronic acid (PBA) with bare **TA-Catechol** in THF solution fails to catch remarkable differences (Figure S19). Intriguingly, adding drops of alkaline aqueous solution activates the **TA-Catechol**/ PBA system shining with bright yellow luminescence under hand-hold UV lamp as shown in Figure 4c. Based on this observation, we optimize the alkalinity and aqueous solution fraction of binary solvent for greatest PL intensity (We have shown the detailed procedure in Supporting Information). Optimization detection conditions are obtained at 1 mM aqueous NaOH solution with fraction of 60%. With these parameters in hand, we acquire series PL spectra of **TA-Catechol**/PBA system with diverse PBA concentrations as shown in Figure 4a. Increasing PBA concentration diminishes the pristine emission band of **TA-Catechol** around 440 nm and

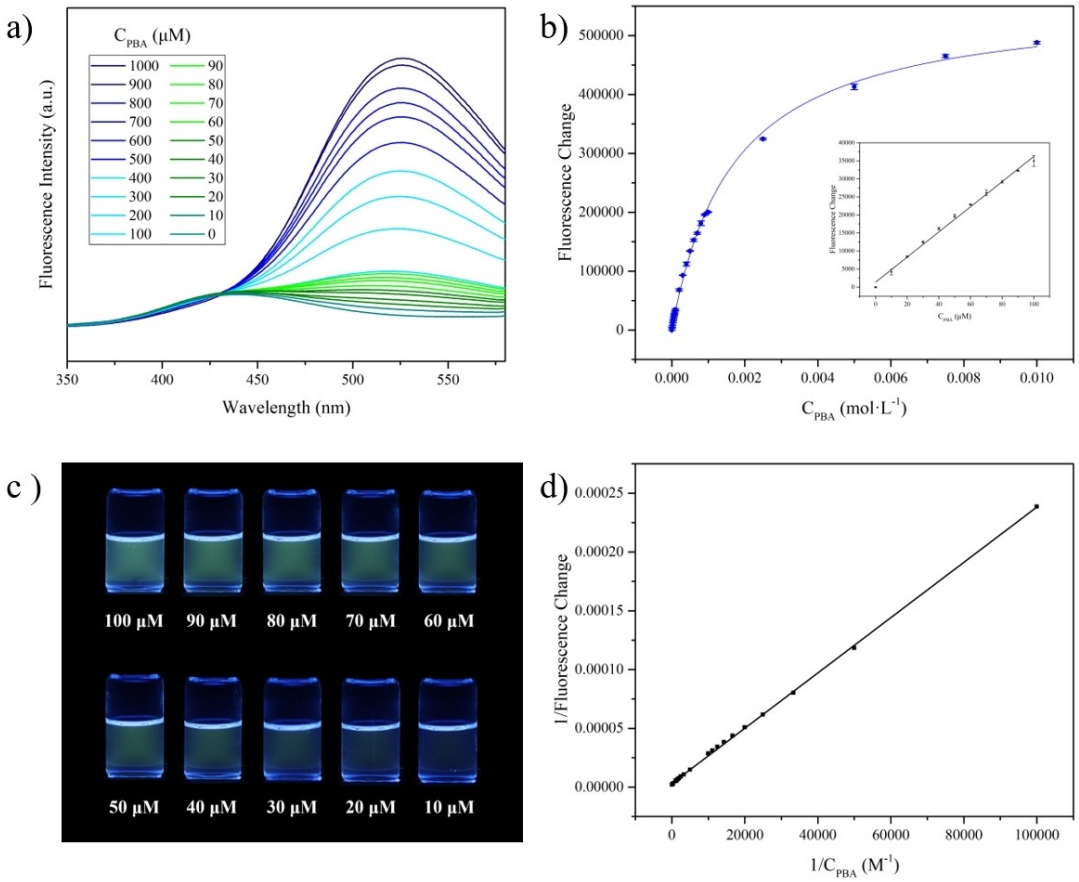

Figure 4. Dual-mode sensing capability of **TA-Catechol** towards PBA. a) Fluorescence spectrum of **TA-Catechol** in alkalescence THF/H_2O binary solvent with varying amounts of PBA. (f_w is controlled at 60% and 1 mM NaOH aqueous solution is utilized). b) Fluorescence change with varying PBA concentrations which is fitted with hyperbola type formula (inset: linear fitting of fluorescence change and PBA concentration at specific condition). c) Photograph of **TA-Catechol** in alkalescence THF/H2O binary solvent with decreasing PBA concentrations. (excited with UV-Lamp of 365 nm). d) Benesi-Hildebrand Plot of the above-mentioned sensing system.

brought about another bathochromic emission band around 530 nm. One isosbestic point located at 430 nm indicates the formation of possible complex species between **TA-Catechol** and PBA within the detection mixture.[26]

Mathematic treatment of the stacked PL spectra renders the calibration-curve of fluorescence change to PBA concentration in Figure 4b. Hypothesizing the formation of **TA-Catechol**/PBA complex which accounts for the yellowish emission, straightforward deduction with proper approximation provides hyperbola type relationship between fluorescence change and PBA concentration which is similar to the legendary Michaelis–Menten equation as follows [Eq. (1)]:[27] (Stepwise deduction could be found in Supporting Information)

$$\Delta FL = (\Delta FL_{max} \times [PBA])/(K_a^{-1} + [PBA]) \quad (1)$$

Non-linear fitting method delivers K_a as 952.38 M^{-1}. The correlation coefficient reaches 99.95% which confirms our assumptions. With PBA: **TA-Catechol** molar ratio inferior to the stoichiometric ratio of 1:1, linear relationship is approximately approached. Linear regression treatment gives the fitting curve of [Eq. (2)]

$$\Delta FL = 348.55 \times [PBA] + 1347.14 \quad (2)$$

The limit of detection (LOD) is estimated as 8.0 μM according to general analytical chemistry method. These results indicate that our probe possesses considerable potential in wide range and quantitative detection of boronic acids. Stability of **TA-Catechol** under the detection condition is also investigated. ^{1}H NMR spectroscopy recorded through 30 days reveals less amount of **TA-Catechol** transforms during a month (Figure S23 and Figure S24). Photoluminescent behavior at varying pH levels is investigated and the optimized detection condition locates at the appropriate pH value while the probe of **TA-Catechol** remains stable (Figure S25 and Figure S26).

Aiming at deepening our understanding towards the sensing procedure, Benesi-Hildebrand Plot[28] is conducted and exhibits linear relationship with correlation coefficient of 99.95% (as shown in Figure 4d). This implies the formation of emissive 1:1 complex between **TA-Catechol** and PBA under the detection condition. Job's Plot shown in Figure 5a further verifies the abovementioned viewpoints and indicates the stoichiometric ratio of **TA-Catechol** over PBA to be 1:1 within the luminescent complex. ^{11}B NMR spectrum is recorded in THF-d_8 with equal molar of **TA-Catechol** and PBA (Figure S27 and Figure S28). It reveals that one fresh boronic species other than PBA emerges while most PBA maintains the status quo. We could hypothesize that straightforward mixing of **TA-Catechol** and PBA in THF affords the tri-coordinated boronic ester inefficiently. Addition of alkaline solution transforms the above boronic ester into the negative charged tetra-coordinated boronic species with one hydroxyl ion coordinating to boron center which may account for the bathochromic emission at around 530 nm. Theoretical methods are utilized to verify our hypothesis. The molecular configuration of tetra-coordinated boronic complex is established and optimized with DFT calculation. Based on this initial molecular model, we analyze the electronic structure of it and find that the vertical excitation energy of postulated complex which could be transformed to theoretical maximum emission wavelength of 578 nm conforms well with our experimental results. Thus, we may conclude that responsibility of **TA-Catechol** towards PBA in this alkalescence THF/H2O binary solvent generates through the formation of tetra-coordinated boronic complex.

Besides, it should be noticed that the **TA-Catechol**/PBA complex displays large stokes shift of almost 230 nm which is quite abnormal. As the experimental spectrum shown in Figure S17, the maximum absorption of **TA-catechol** and **TA-Catechol**/PBA complex is almost at the same wavelength of about 300 nm, while the bathochromic shifted emission emerges at the **TA-Catechol**/PBA complex. To figure out this

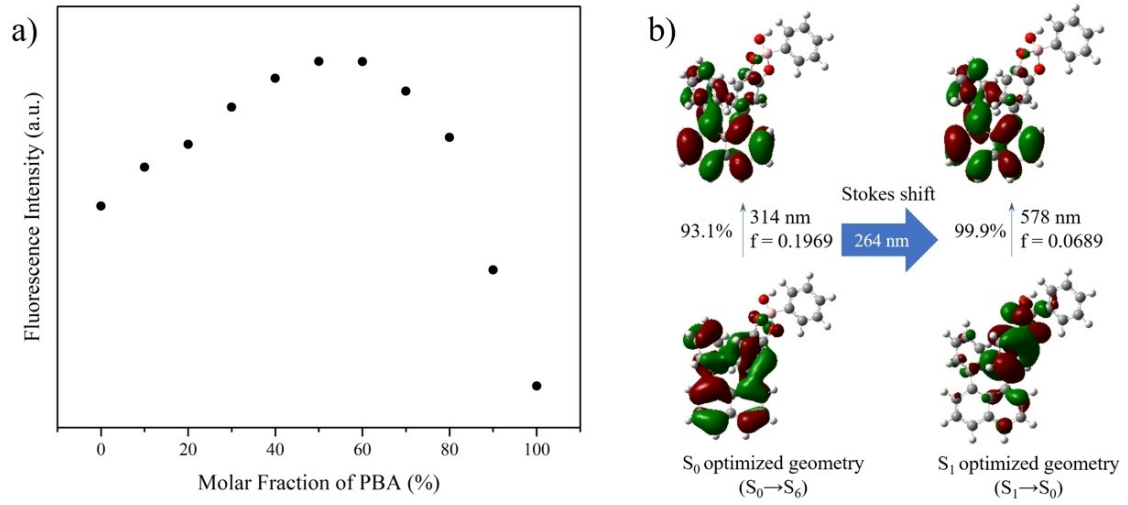

Figure 5. Mechanistic discussions of the detection procedure. a) Job's Plot with varying molar fraction of PBA. b) Natural transition orbitals (NTOs) of predicted **TA-catechol**/PBA complex.

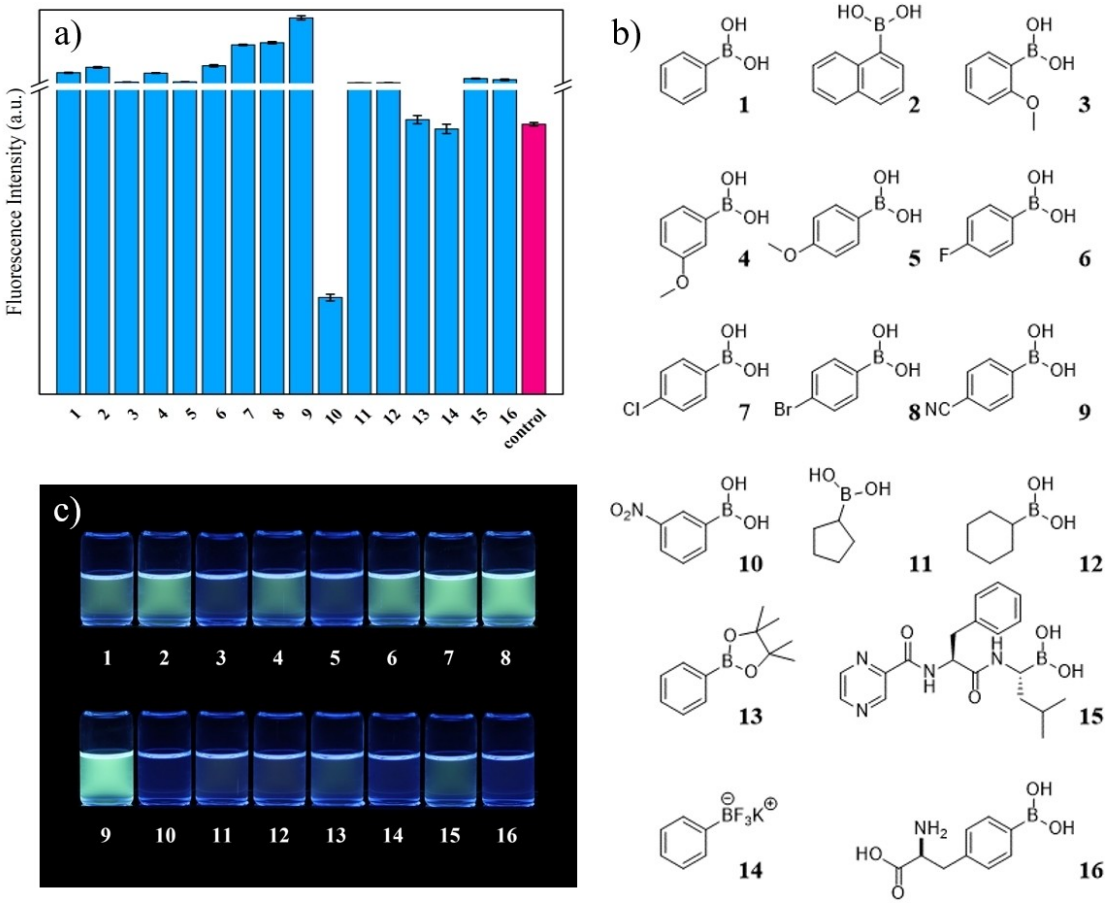

Figure 6. Responsibility of **TA-Catechol** towards diverse boronic acids. a) Fluorescence intensity of **TA-Catechol** with several boronic species under optimal detection condition. b) List of investigated organic boronic species. c) Photograph of **TA-Catechol** with listed boronic species. (excited with UV-Lamp of 365 nm).

experimental result, we study the transition of the S_0 and S_1 optimized geometry of **TA-Catechol** and the predicted emissive structure of **TA-Catechol**/PBA complex. For absorption spectrum, the vertical excitation energy, transitions, oscillator strengths and frontier orbitals at S_0 optimized geometries are listed in Table S4-S7. With identification of the strongest oscillator strength as the main absorption process, we may conclude that the absorption of **TA-Catechol** is attributed to the $S_0 \rightarrow S_2$ transition at 314 nm while the absorption of predicted emissive compound of **TA-Catechol** and PBA comes from $S_0 \rightarrow S_6$ transition at the same wavelength. What's more, the natural transition orbitals (NTOs) show the similar transition localized in the **TA-Catechol** but not the PBA derives (Figure 5b and Figure S33), which further verifies the similar absorption among two systems. However, the emission process is quite different because of varied $S_1 \rightarrow S_0$ transition at S_1 optimized geometry. The predicted emissive compound of **TA-Catechol** with PBA is much related to the catechol phenyl group in the highest occupied NTO (HONTO) while the lowest unoccupied NTO (LUNTO) remains at 8-phenyl naphthalene structure. This significant intramolecular through-space charge transfer (ICT) character within **TA-catechol**/PBA complex accounts for the larger stokes shift of **TA-Catechol**/PBA complex than the pristine **TA-Catechol**.

Large stokes shift of the emissive **TA-Catechol**/PBA complex brings about conspicuous yellow luminescence. As scientists have illustrated that human eye is most sensitive to yellowish-green color[29] which coincidently agrees with the emission wavelength of **TA-Catechol**/PBA complex here. Thus, visual detection capability is examined with gradient PBA concentration. As shown in Figure 4c, distinct contrast could be grasped with naked eyes while the minimum PBA concentration to be distinguished via visual detection mode is caught at 10 μM. This value is almost closed to the LOD of the quantitative mode.

Analyte scope of diverse boronic acids

Systematic discussion of the recognition process between **TA-Catechol** and PBA stimulates our interest in other organic small-molecules containing boronic acid functional groups. Series of organic boronic acids covering both aliphatic and aromatic ones **1**–**12** are selected to our sensing system. Boronic ester **13** and trifluoroborate salt **14** are adopted for comparison.

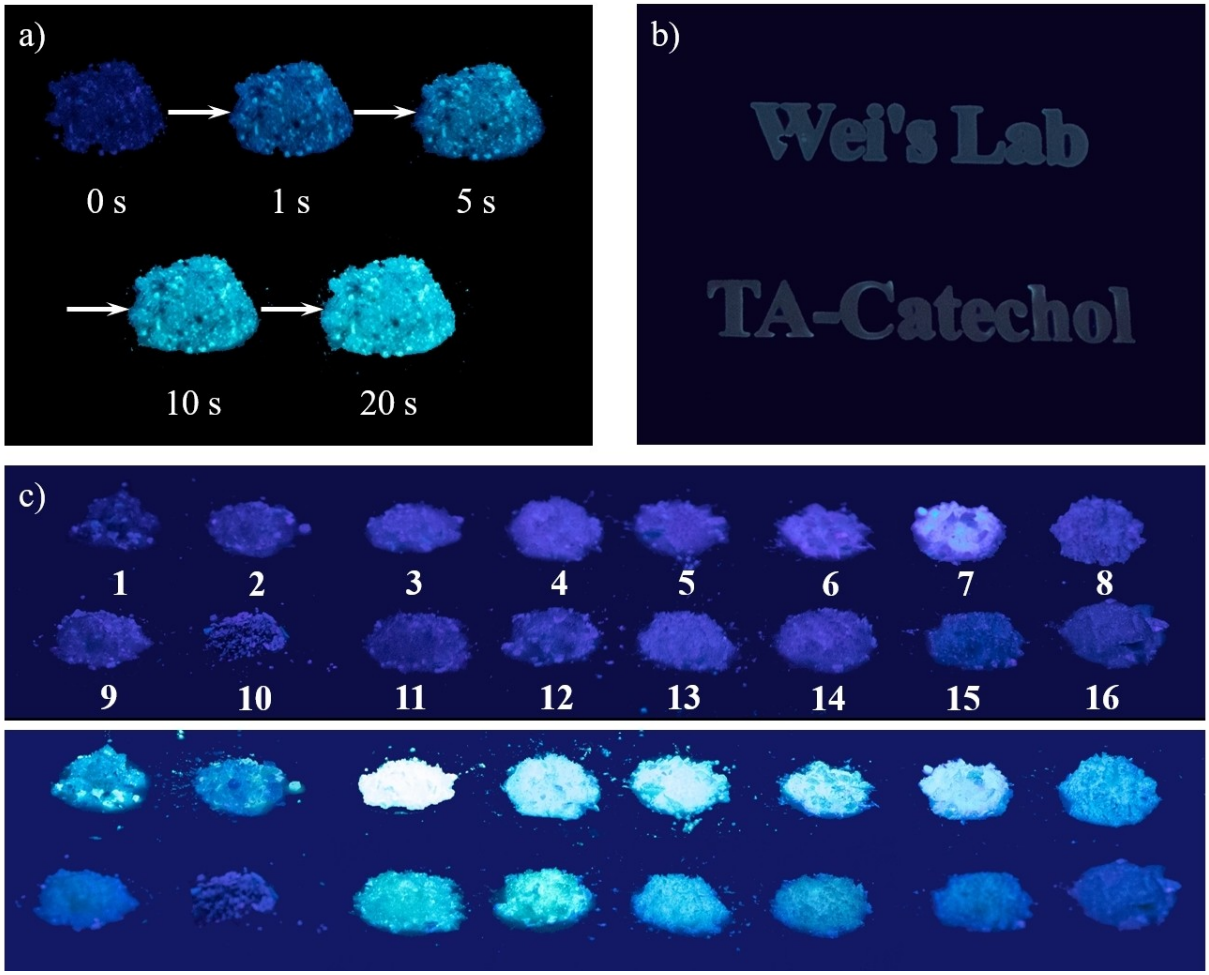

Figure 7. Solid-state recognition based on **TA-Catechol** and boronic acids. (excited with UV-Lamp of 365 nm) a) Photograph of **TA-Catechol**/PBA mixture under NEt_3 atmosphere with increasing exposure time. b) Photograph of patterns composed of **TA-Catechol**/PBA mixture through NEt_3 fuming. c) Photograph of boronic species listed in Figure 6b with **TA-Catechol**. (the upper half part is observed under ambient condition while the lower half part observed in NEt_3 atmosphere).

The commercialized anti-tumor drug Bortezomib[30] **15** and Boron Neutron Capture Therapy (BNCT) involved delivery agent p-boronophenylalanine (BPA)[31]**16** are selected to evaluate the practical detection capability. As shown in Figure 6a, **TA-Catechol** almost responds to any analytes among our list except the nitro-substituted one under optimal detection condition. Visual detection mode demonstrated in Figure 6c also displays versatile detection capability of **TA-Catechol** towards diverse boronic species.

With the verified large detection capacity among organic boronic acids, high throughput screening based on photo-luminescent method is conceivable. For instance, we could exploit this tri-aryl type fluorescent luminogen in screening for optimal reagent composition and reaction conditions among synthetic methodologies involving boronic species with the high throughput manner. In addition, this fluorescent sensor might deliver new insights into drug metabolism research associated with boron-containing drugs.

Potential applications based on solid-state recognition

Solid-state fluorescence probes hold numerous advantages including environmentally-benign, processable and recyclable. However, this remains a great challenge for conventional luminogens on account of the exhausting aggregation-caused quenching (ACQ) effect. In this work, the AIE feature of **TA-Catechol** endows it with tremendous potential in solid-state applications. Based on the sensing mechanism proposed above, we envision that replaces the hydroxyl ion with nitrogenous ligand in the tetra-coordinated boronic species may also generate one luminescent intermediate. This leads to the attempt of solid-state recognition towards boronic acids with **TA-Catechol** under NEt_3 atmosphere. To be exact, equal molar amount of **TA-Catechol** and PBA is mixed uniformly with several minutes of milling. As shown in Figure 7a, the mixture of **TA-Catechol** and PBA emits bluish violet luminescence under ambient condition. Fuming with NEt_3 results in rapid color change under UV irradiation within 1 s, further storage inside the NEt_3 atmosphere turns the emission color to greenish

yellow. About 20 seconds later, the solid color remains unchanged under UV irradiation. This rapid solid-state recognition process stimulates multiple potential applications. As shown in Figure 7b, predesigned patterns composed of **TA-Catechol** and PBA mixture are arranged on a silica gel plate, fuming with NEt_3 renders it shining with greenish yellow luminescence. This may open up a fresh avenue for construction of future cryptosystem.[32] The feasibility of this solid-state recognition pathway of diverse boronic species is also examined in Figure 7c. We find that almost each boronic containing molecule in Figure 6b exhibits bathochromic shifted emission on mixing with **TA-Catechol** in NEt_3 atmosphere. This would bring about feasible protocol for solid-state boronic acid detection, relevant work is being conducted in our laboratory and results would be reported later.

Conclusion

Novel tri-aryl type AIEgen bearing catechol moiety has been designed and synthesized via intrinsic functionalization strategy in this work. The pristine luminogen **TA-Catechol** shows typical AIE behavior which could be explained comprehensively with theoretical methods. In alkalescence THF/H_2O solution, **TA-Catechol** exhibits rapid recognition property towards diverse organic boronic acids. Visual and quantitative detection mode is implemented, the LOD of the quantitative procedure is down to 8.0 μM while the visual resolution limit approaches 10 μM. Sensing mechanism is proposed with the hypothesis of a luminescent tetra-coordinated boronic species which is formed under the optimal detection condition. Control experiments and theoretical calculations find results satisfying our assumptions. Diverse organic boronic acids are compatible with our sensing system and the solid-state recognition capability is also illustrated. The rapid, precise and convenient detection procedure with novel luminogen of **TA-Catechol** is highly promising in high throughput screening and pharmaceutical research.

X-ray crystallography

Deposition Number(s) 2077157 (for TA-Catechol) contain(s) the supplementary crystallographic data for this paper. These data are provided free of charge by the joint Cambridge Crystallographic Data Centre and Fachinformationszentrum Karlsruhe Access Structures service.

Acknowledgements

This work was supported by the National Natural Science Foundation of China (Nos. 21788102 and 24174057). We are most grateful to Hongye Huang, Liucheng Mao, Danning Hu, Yuanheng Wang and Prof. Lei Tao of Tsinghua University for valuable suggestions.

Conflict of Interest

The authors declare no conflict of interest.

Keywords: boronic acid recognition · catechol moiety · dual-mode detection · functional AIEgen · tetra-coordinated boron

[1] a) K. Smith, in *Organometallics in Synthesis: A Manual*, Wiley, Chichester, West Sussex, England, **2001**, p. 465; b) *From Little Acorns to Tall Oaks-from Boranes through Organoboranes* (Nobel Lecture), H. C. Brown, **1979**, http://www.nobelprize.org/.
[2] a) N. Miyaura, A. Suzuki, *Chem. Rev.* **1995**, *95*, 2457; b) N. Miyaura, A. Suzuki, *J. Chem. Soc. Chem. Commun.* **1979**, 866; c) N. Miyaura, K. Yamada, A. Suzuki, *Tetrahedron Lett.* **1979**, *20*, 3437.
[3] D. G. Hall, in *Boronic Acids: Preparation, Applications in Organic Synthesis and Medicine*, Wiley, Boschstr, Weinheim, Germany **2010**.
[4] a) B. S. L. Collins, C. M. Wilson, E. L. Myers, V. K. Aggarwal, *Angew. Chem. Int. Ed.* **2017**, *56*, 11700; *Angew. Chem.* **2017**, *129*, 11860; b) J. W. B. Fyfe, A. J. B. Watson, *Chem* **2017**, *3*, 31; c) C. Shu, A. Noble, V. K. Aggarwal, *Nature* **2020**, *586*, 714; d) P. Zheng, P. Zhou, D. Wang, W. Xu, H. Wang, T. Xu, *Nat. Commun.* **2021**, *12*, 1646; e) Y. Yang, J. Tsien, A. Ben David, J. M. E. Hughes, R. R. Merchant, T. Qin, *J. Am. Chem. Soc.* **2021**, *143*, 471.
[5] a) P. C. Trippier, C. McGuigan, *MedChemComm* **2010**, *1*, 183; b) G. F. S. Fernandes, W. A. Denny, J. L. Dos Santos, *Eur. J. Med. Chem.* **2019**, *179*, 791.
[6] R. F. Barth, P. Mi, W. Yang, *Cancer Commun.* **2018**, *38*, 35.
[7] a) T. D. James, K. R. A. S. Sandanayake, S. Shinkai, *Angew. Chem. Int. Ed.* **1996**, *35*, 1910; *Angew. Chem.* **1996**, *108*, 2038; b) T. D. James, P. Linnane, S. Shinkai, *Chem. Commun.* **1996**, 281.
[8] Y. Guan, Y. Zhang, *Chem. Soc. Rev.* **2013**, *42*, 8106.
[9] C. Flender, P. Leonhard, C. Wolf, M. Fritzsche, M. Karas, *Anal. Chem.* **2010**, *82*, 4194.
[10] X. Wang, D. Yue, E. Lv, L. Wu, W. Qin, *Anal. Chem.* **2014**, *86*, 1927.
[11] a) W. Wang, G. Springsteen, S. Gao, B. Wang, *Chem. Commun.* **2000**, 1283; b) T. E. Barder, S. L. Buchwald, *Org. Lett.* **2007**, *9*, 137; c) M. R. Aronoff, B. VanVeller, R. T. Raines, *Org. Lett.* **2013**, *15*, 5382.
[12] J. Lim, D. Nam, O. Š. Miljanić, *Chem. Sci.* **2012**, *3*, 559.
[13] H. O. House, R. W. Magin, H. W. Thompson, *J. Org. Chem.* **1963**, *28*, 2403.
[14] H. O. House, W. J. Campbell, M. Gall, *J. Org. Chem.* **1970**, *35*, 1815.
[15] R. L. Clough, J. D. Roberts, *J. Am. Chem. Soc.* **1976**, *98*, 1018.
[16] F. Cozzi, M. Cinquini, R. Annunziata, T. Dwyer, J. S. Siegel, *J. Am. Chem. Soc.* **1992**, *114*, 5729.
[17] a) A. Tsurusaki, T. Sasamori, A. Wakamiya, S. Yamaguchi, K. Nagura, S. Irle, N. Tokitoh, *Angew. Chem. Int. Ed.* **2011**, *50*, 10940; *Angew. Chem.* **2011**, *123*, 11132; b) S. Bontemps, M. Devillard, S. Mallet-Ladeira, G. Bouhadir, K. Miqueu, D. Bourissou, *Inorg. Chem.* **2013**, *52*, 4714.
[18] C. Wolf, X. Mei, *J. Am. Chem. Soc.* **2003**, *125*, 10651.
[19] a) X. Mei, C. Wolf, *J. Am. Chem. Soc.* **2004**, *126*, 14736; b) X. Mei, C. Wolf, *J. Am. Chem. Soc.* **2006**, *128*, 13326; c) M. W. Ghosn, C. Wolf, *J. Am. Chem. Soc.* **2009**, *131*, 16360; d) K. W. Bentley, C. Wolf, *J. Org. Chem.* **2014**, *79*, 6517.
[20] a) X. You, G. Zhang, C. Zhan, Y. Wang, D. Zhang, in *Aggregation-Induced Emission: Materials and Applications Volume 2*, Vol. 1227, American Chemical Society **2016**, Ch. 4, p. 93; b) M. Gao, B. Z. Tang, *ACS Sens.* **2017**, *2*, 1382; c) J. Mei, N. L. C. Leung, R. T. K. Kwok, J. W. Y. Lam, B. Z. Tang, *Chem. Rev.* **2015**, *115*, 11718; d) J. Yang, Z. Chi, W. Zhu, B. Z. Tang, Z. Li, *Sci. China Chem.* **2019**, *62*, 1090.
[21] M. Wang, Y. Wang, R. Hu, J. Yuan, M. Tian, X. Zhang, Z. Shuai, Y. Wei, *Commun. Chem.* **2021**, *4*, 55.
[22] S. Kaneko, S. Yotoriyama, H. Koda, S. Tobita, *J. Phys. Chem. A* **2009**, *113*, 3021.
[23] M. J. Frisch, G. W. Trucks, H. B. Schlegel, G. E. Scuseria, M. A. Robb, J. R. Cheeseman, G. Scalmani, V. Barone, G. A. Petersson, H. Nakatsuji, X. Li, M. Caricato, A. V. Marenich, J. Bloino, B. G. Janesko, R. Gomperts, B. Mennucci, H. P. Hratchian, J. V. Ortiz, A. F. Izmaylov, J. L. Sonnenberg, Williams, F. Ding, F. Lipparini, F. Egidi, J. Goings, B. Peng, A. Petrone, T. Henderson, D. Ranasinghe, V. G. Zakrzewski, J. Gao, N. Rega, G. Zheng, W. Liang, M. Hada, M. Ehara, K. Toyota, R. Fukuda, J. Hasegawa, M. Ishida, T. Nakajima, Y. Honda, O. Kitao, H. Nakai, T. Vreven, K. Throssell, J. A. Montgomery Jr., J. E. Peralta, F. Ogliaro, M. J. Bearpark, J. J. Heyd, E. N. Brothers, K. N. Kudin, V. N. Staroverov, T. A. Keith, R. Kobayashi, J. Normand, K. Raghavachari, A. P. Rendell, J. C. Burant, S. S. Iyengar, J.

Tomasi, M. Cossi, J. M. Millam, M. Klene, C. Adamo, R. Cammi, J. W. Ochterski, R. L. Martin, K. Morokuma, O. Farkas, J. B. Foresman, D. J. Fox, Wallingford, CT **2016**.
[24] a) Z. Shuai, Q. Peng, *Phys. Rep.* **2014**, *537*, 123; b) Z. Shuai, Q. Peng, *Natl. Sci. Rev.* **2016**, *4*, 224; c) Y. Niu, W. Li, Q. Peng, H. Geng, Y. Yi, L. Wang, G. Nan, D. Wang, Z. Shuai, *Mol. Phys.* **2018**, *116*, 1078; d) S. Lin, Q. Peng, Q. Ou, Z. Shuai, *Inorg. Chem.* **2019**, *58*, 14403.
[25] a) J. Yang, M. A. Cohen Stuart, M. Kamperman, *Chem. Soc. Rev.* **2014**, *43*, 8271; b) Y. Suzuki, D. Kusuyama, T. Sugaya, S. Iwatsuki, M. Inamo, H. D. Takagi, K. Ishihara, *J. Org. Chem.* **2020**, *85*, 5255.
[26] M. D. Cohen, E. Fischer, *J. Chem. Soc. (Resumed)* **1962**, 3044.
[27] D. L. Nelson, A. L. Lehninger, M. M. Cox, in *Lehninger principles of biochemistry*, Macmillan, **2008**.
[28] a) H. A. Benesi, J. H. Hildebrand, *J. Am. Chem. Soc.* **1949**, *71*, 2703; b) M. Barra, C. Bohne, J. C. Scaiano, *J. Am. Chem. Soc.* **1990**, *112*, 8075.
[29] G. Wald, *J. Opt. Soc. Am.* **1945**, *35*, 187.
[30] A. Paramore, S. Frantz, *Nat. Rev. Drug Discovery* **2003**, *2*, 611.
[31] Y. Mishima, C. Honda, M. Ichihashi, H. Obara, J. Hiratsuka, H. Fukuda, H. Karashima, T. Kobayashi, K. Kanda, K. Yoshino, *Lancet* **1989**, *334*, 388.
[32] J. Ji, D. Hu, J. Yuan, Y. Wei, *Adv. Mater.* **2020**, *32*, 2004616.

Manuscript received: September 14, 2021
Accepted manuscript online: November 8, 2021
Version of record online: November 23, 2021